POLISH MARITIME RESEARCH 2 (130) 2026 Vol. 33; pp. 64-73
10.2478/pomr-2026-0021

Application Performance of Synthetic Fibre Ropes in Marine Towing Systems

He Zhang [1,*]
Ji Zeng [2]
Bowen Jin [1]
Chiate Chou [3]
Hailei Dong [3]
Hangyu Li [3]
[1] Merchant Marine College, Shanghai Maritime University, Shanghai, China
[2] College of Ocean Science and Engineering, Shanghai Maritime University, Shanghai, China
[3] Zhejiang Four Brothers Rope Co., Ltd., Zhejiang, China

* Corresponding author: *zhanghe_mu@163.com (He Zhang)*

ABSTRACT

A multi-body coupled mathematical model of a tug–barge–rope system is developed to address the absence of comprehensive parameter design theories for synthetic fibre ropes in marine towing systems and the challenges associated with stability regulation under complex sea states. This study systematically examines the effects of three rope lengths (20, 80, and 120 m) and three fibre materials (nylon, polyester, and ultra-high-molecular-weight polyethylene) on the dynamic performance of a towing system. The mechanical coupling relationships between system components are explored by utilising a dynamic control model. Parametric analysis highlighted the mechanical properties, elongation deformation, and stiffness evolution of ropes of varying lengths and materials during towing operations. The results indicate that short ropes demonstrate high strain sensitivity and instantaneous stiffness, which can readily induce overloads in the power system of the tug. Medium-length ropes, benefiting from viscoelastic deformation, facilitate energy dissipation, thereby mitigating tension fluctuations and enhancing motion stability. In contrast, long ropes result in delayed barge responses owing to stiffness attenuation. This study also revealed that different fibre materials offer distinct advantages in terms of force transmission, vibration suppression, and load-bearing capacity. Based on model analysis and a parametric study, optimal selection schemes for synthetic fibre ropes are proposed. The findings provide a theoretical foundation and practical guidance for the performance optimisation and engineering application of synthetic fibre ropes in marine towing systems, contributing significantly to the advancement of ocean engineering.

Keywords: synthetic fibre rope; marine towing system; rope length; fibre material; mechanical properties

INTRODUCTION

Marine towing systems are essential in ocean engineering, maritime rescue, and port operations, influencing the efficiency and success of offshore activities through operational safety and cost-effectiveness. Within the power transmission chain connecting the tug and barge, such as drilling platforms, engineering barges, and large marine equipment, the rope serves as the primary medium for force and motion transmission (Fig. 1). The mechanical performance and dynamic response properties determine the overall stability of the towing system. Advancements in materials engineering have led to the widespread adoption of synthetic fibre ropes, which offer significant advantages over conventional steel wires, including high strength, low areal density, superior corrosion resistance, and enhanced flexibility. These attributes have established synthetic fibre ropes as the preferred choice in modern marine towing systems. Consequently, optimising their performance is crucial for enhancing operational efficiency in ocean engineering.

Fig. 1 Application of synthetic fibre ropes in marine towing operations

Synthetic fibre ropes show complex, load-dependent mechanical behaviours that are critical for marine engineering applications. These include rate-dependent dynamic stiffness, time-varying viscoelastic deformation with hysteretic energy dissipation, stress-accelerated creep rupture, and cyclic fatigue. Such inherent characteristics are sensitive to external loading conditions and material microstructures, and directly determine the dynamic response, force transmission efficiency, and long-term structural stability of marine systems. Specifically, Ma et al. [1] identified creep and abrasion as the dominant failure modes of polyester yarns under different loads. Based on experimental investigations, Zhang et al. [2] quantified the nonlinear dynamic stiffness evolution of polyester mooring ropes and revealed the energy dissipation mechanism induced by viscoelasticity, which is consistent with the experimental findings of Lian [3], who conducted in-depth research on the dynamic stiffness of full-scale polyester mooring ropes. Meanwhile, Kontou et al. [4] developed a nonlinear viscoelastic/viscoplastic constitutive model, providing a theoretical foundation for describing the time-dependent mechanical response of fibre ropes. Furthermore, Zhang et al. [5] established empirical formulas for the stiffness evolution of deep-sea mooring ropes under long-term cyclic loads and idle periods, linking macroscopic mechanical behaviour to engineering design. Recent experimental studies by Xie et al. [6] have further supplemented our understanding of synthetic fibre rope mechanics, as they systematically investigated the quasi-static and dynamic stiffness of full-scale HMPE ropes, enriching the experimental data for the mechanical analysis of marine towing system ropes. In addition, Wu et al. [7] highlighted that fibre ropes present distinctly different dynamic characteristics from traditional rigid mooring components, which significantly affects the stability of floating marine structures.

Previous theoretical academic research systematically explored the nonlinear mechanical behaviour and stability mechanisms of towing systems, providing a foundation for the engineering applications of synthetic fibre ropes. Bernitsas and Kekridis [8] developed a fundamental theoretical framework for towing system dynamics through numerical simulation and stability analyses of ship towing operations, elucidating the core parameters and boundary conditions of rope mechanics modelling. Focusing on the nonlinear dynamics of a barge using elastic ropes, subsequent research [9] elucidated the role of the elastic properties of fibre ropes in modulating the dynamic responses of towing systems. They quantitatively established the intrinsic correlation between the elastic modulus of synthetic fibre materials and the stability domain of the system. Focusing on barge towing systems, Lee [10] further advanced analytical methods for evaluating nonlinear dynamic stability. Through comparative experiments, they demonstrated the significant advantage of synthetic fibre ropes to absorb impact loads during large-scale barge towing operations. Bernitsas and Chung [11] investigated the nonlinear stability of dual-rope towing and mooring systems, analysed the load distribution characteristics of synthetic fibre ropes under multi-rope cooperative configurations, and provided theoretical guidance for rope selection and configuration in complex towing scenarios. Collectively, these studies established a theoretical framework for comprehending the mechanical behaviour of synthetic fibre ropes in towing systems, emphasising the coupling between material properties and system stability.

In terms of environmental adaptability, research has increasingly focused on wind load interference and the adaptation to diverse material properties. Kijima and Varyani [12] and Fitriadhy et al. [13] systematically investigated the mechanisms by which wind loads disturb course stability in dual-tug and single-ship towing systems, respectively, utilising wind tunnel experiments and numerical simulations. Their findings revealed that the flexibility of synthetic fibre ropes enables them to buffer wind-induced perturbations through dynamic deformation. However, the deformation amplitude is dependent on the stiffness parameters: insufficient stiffness can result in significant heading deviations; whereas, excessive stiffness reduces buffering effectiveness. Recent research has focused on material diversity in synthetic fibre ropes. Huang et al. [14] conducted comparative analyses of the stress–strain responses and fatigue damage evolution of typical fibre materials, such as polyester and aramid, under wind loads. Their research provided valuable data for material selection under varying wind conditions, advancing the understanding of the interplay between material properties and environmental adaptability in synthetic fibre ropes. These findings offer significant insights for the design of towing systems in complex meteorological conditions.

Regarding engineering applications and optimisation practices, research has increasingly concentrated on the practical deployment of technology in specific operational scenarios and enhancements in efficiency. Regarding the wet towing of floating bodies (which is a critical scenario), Cao et al. [15] systematically summarised the factors influencing the stability of towed floaters. They emphasised that the coupling between the mechanical properties of rope and floater dynamic responses is crucial for operational safety, providing a theoretical framework for the design of the towing scheme of large floaters, such as offshore wind platforms. Regarding offshore wind turbine towing, Roberts et al. [16] investigated the IEA 15 MW turbine on the UMaine VolturnUS-S floating platform. Through scale-model tests and ship-simulator simulations, they validated the reliability of synthetic fibre ropes in towing ultra-large floating bodies. The lightweight nature of these ropes reduces the power demand on tugs; whereas, their high strength ensures safe transmission under extreme conditions, significantly lowering towing energy consumption. By innovatively integrating intelligent algorithms, such as genetic algorithms and multi-objective evolutionary optimisation into scheme design, and by embedding critical material parameters, including the fatigue life and wind-induced deformation limits of synthetic fibre ropes, into routing and scheduling models, recent studies have developed optimisation pathways that synchronise material property constraints with operational efficiency enhancement [17–20]. This approach has significantly advanced the precise application of synthetic fibre ropes in practical towing operations.

However, two fundamental challenges continue to impede the engineering application of synthetic fibre ropes in marine towing systems. First, in essential areas, such as rope length selection and multi-rope cooperative load distribution, systematic theoretical support and quantitative methods are lacking. This can result in excessive elongation (exacerbating fatigue damage) or unnecessary strength redundancy, which results in increased costs and diminished operational flexibility. Second, under complex sea conditions, such as coupled wind–wave–current conditions, the nonlinear mechanical characteristics of synthetic fibre ropes, such as viscoelasticity and lag effects, combine with dynamic elastic deformation, complicating the precise regulation of towing system stability and elevating operational risks. Consequently, performance evaluation studies of synthetic fibre ropes in marine towing systems have become essential for overcoming these bottlenecks. Accurately quantifying the effect of rope length and material properties on the dynamic characteristics of towing systems is essential for advancing system control models, enhancing the stability and reliability of towing operations, and providing scientific guidance for rope selection and structural design. This research holds both theoretical and engineering significance.

This study focused on evaluating the application performance of synthetic fibre ropes in marine towing systems. A comprehensive multi-body coupled mathematical model of a tug–barge–rope system was developed to elucidate the elongation deformation patterns, tension transmission properties, and stiffness evolution mechanisms of synthetic fibre ropes of varying materials and lengths during towing operations.

This study has three main components. Firstly, a dynamic control model of the rope–towing system was established, clarifying the mechanical coupling relationships among system components and providing a robust theoretical framework for subsequent performance analyses. Secondly, parametric studies were conducted using the developed model. These studies examined the influence of the rope length on the dynamic performance of the towing system, including stability margins and dynamic response characteristics across different lengths. The regulatory patterns of rope fibre materials in system dynamics were also investigated, identifying the regulatory mechanisms and application advantages of different materials and delineating their optimal use scenarios. Finally, by integrating the results of the model analysis and parametric studies, selection schemes were developed for the optimised application of synthetic fibre ropes in marine towing systems. These schemes provide a robust theoretical foundation and practical technical guidance for engineering applications. The findings of this study are anticipated to facilitate performance optimisation and promote the wider adoption of synthetic fibre ropes in marine towing systems, contributing to the high-quality advancement of ocean engineering.

CONTROL MODEL OF THE ROPE TOWING SYSTEM

To establish a concise mathematical representation of the rope towing system, the six degrees of freedom (DoF) ship model was reduced to three DoFs by neglecting heave, roll, and pitch motions, and considering only surge, sway, and yaw. The basic model of the barge and its force distribution are shown in.

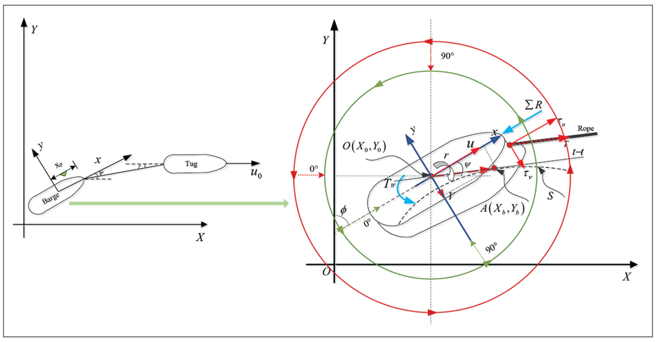

Fig. 2 Numerical model of a barge in the X–Y coordinate system

The inertial and fixed-body coordinate systems are defined as *OXY* and *oxy*, respectively. In the inertial *X*-*Y* system, only translational motions along the *X* and *Y*-axes, as well as rotational motion about the heading direction, are considered. Here, *S* denotes the trajectory of the ship; point $O(X_0, Y_0)$ represents the position of the centre of mass of the ship; the direction of motion is defined by the line *t*-*t*, which passes through the centre of mass of the ship and tangent point $A(X_b, Y_b)$ of the trajectory; ψ represents the course angle of the ship; ϕ represents the yaw angle of the ship; u, v, and r represent the surge, sway, and yaw angular velocities, respectively; T represents the rope tension acting on the hull; τ_u and τ_r represent the components of the rope tension T along the body-fixed x and y-axes; T_w represents the rotational resistance moment of the hull; and ΣR denotes the total resistance force acting on the ship. The numerical equations for the tug and barge are expressed as follows:

$$\begin{cases} \dot{\eta}_i = J(\eta_i)v_i \\ M_i\dot{v}_i + C_i(v_i)v_i + D_i(v_i)v_i = \tau_i \pm T_{cable} \end{cases} \quad (1)$$

where i denotes the ship type, with $i = 1$ representing the tug and $i = 2$ representing the barge; η represents the position vector of the ship; v represents the velocity vector of the ship; M represents the added mass matrix of the ship; C represents the Coriolis and centripetal matrix; D represents the damping matrix; τ represents the external forces acting on the tug and barge (including environmental forces); and T_{rope} represents the rope force.

The terms M, $C(v)$, and D in Eq. (1) can be simplified as follows [1]:

$$M = \begin{bmatrix} m_{11} & 0 & 0 \\ 0 & m_{22} & m_{23} \\ 0 & m_{22} & m_{23} \end{bmatrix} = \begin{bmatrix} m - X_{\dot{u}} & 0 & 0 \\ 0 & m - X_{\dot{v}} & mx_g - Y_{\dot{r}} \\ 0 & mx_g - N_{\dot{v}} & I_z - N_{\dot{r}} \end{bmatrix} \quad (2)$$

$$C(v)=\begin{bmatrix}0 & 0 & C_{13}\\ 0 & 0 & C_{23}\\ -C_{13} & -C_{13} & 0\end{bmatrix}=$$

$$\begin{bmatrix}0 & 0 & m_{22}v-\frac{m_{23}+m_{32}}{2}r\\ 0 & 0 & m_{11}u\\ m_{22}v+\frac{m_{23}+m_{32}}{2}r & -m_{11}u & 0\end{bmatrix} \tag{3}$$

$$D=\begin{bmatrix}D_{11} & 0 & 0\\ 0 & D_{22} & D_{23}\\ 0 & D_{32} & D_{33}\end{bmatrix}=$$

$$\begin{bmatrix}-(X_u+X_{|u|u}|u|) & 0 & 0\\ 0 & -(Y_v+Y_{|v|v}|v|+Y_{|r|v}|r|) & -(Y_r+Y_{|v|r}|v|)\\ 0 & -(N_v+N_{|v|v}|v|+N_{|r|v}|r|) & -(N_r+N_{|v|r}|v|+N_{|r|v}|r|)\end{bmatrix} \tag{4}$$

Adopting the concept of decoupled modelling, the body-fixed coordinate system is defined at the centre of mass of the ship, where $x_g = 0$, m denotes the mass of the ship, T_z represents the moment of inertia about the z-axis, $X_{\dot{u}}$, $Y_{\dot{v}}$, and $N_{\dot{r}}$ represent the added mass coefficients in surge, sway, and yaw, respectively, $Y_{\dot{r}}$ and $N_{\dot{v}}$ represent the cross-coupling added mass coefficients, X_u, Y_v, Y_r, N_v, and $N_{\dot{r}}$ represent the linear damping coefficients, and $X_{|u|u}$, $Y_{|v|v}$, $Y_{|r|v}$, $Y_{|v|r}$, $N_{|v|v}$, $N_{|r|v}$, $N_{|v|r}$, and $N_{|r|r}$ represent the nonlinear damping coefficients. The equations governing the ship motion are subsequently derived [21]. In Eq. (1), $\eta_i = [x_i\ y_i\ \psi_i]^T$ and $v_i = [u_i\ v_i\ r_i]^T$, where $i = b, t$ represent the barge and tug, respectively. The relationship between $\dot{\eta}_i$ and v_i is expressed as follows:

$$\dot{\eta}_i=\begin{bmatrix}\dot{x}_i\\ \dot{y}_i\\ \dot{\psi}_i\end{bmatrix}=\begin{bmatrix}\cos\psi_i & -\sin\psi_i & 0\\ \sin\psi_i & \cos\psi_i & 0\\ 0 & 0 & 1\end{bmatrix}\begin{bmatrix}u_i\\ v_i\\ r_i\end{bmatrix} \tag{5}$$

The tension exerted by the towing rope is expressed as follows:

$$\begin{cases}T_x = T\cos(\gamma+\psi)\\ T_y = T\sin(\gamma+\psi)\\ M_x = Tx_p\sin(\gamma+\psi)\end{cases} \tag{6}$$

where T represents the rope tension; x_p denotes the longitudinal coordinate of the towing point relative to the centre of gravity of the ship; ψ represents the yaw angle of the ship; and γ represents the angle between the rope and translational direction of the barge. The nonlinear relationship between rope tension and elongation can be calculated by utilising a spring–damper model, as follows:

$$T = K_r \cdot \Delta L \tag{7}$$

K_r represents the nonlinear stiffness of the rope, which varies with elongation (Eq. (5)), and $\Delta L = l - l_0$ represents the elongation of the rope. Furthermore, l and l_0 represent the current and original lengths, respectively. When $l < l_0$, i.e. when the rope is slack, $T = 0$.

$$K_r\begin{cases}K_{r_0}(1+\delta\cdot\varepsilon) & l > l_0\\ 0 & l \le l_0\end{cases} \tag{8}$$

where K_{r_0} represents the initial stiffness of the rope; δ represents the nonlinear stiffness coefficient; and ε represents the relative strain, defined as the ratio of rope elongation to its original length, $\varepsilon = \Delta L / l_0$.

Redundant terms in the ship model can be eliminated and simplified. The three DoF geometric kinematic equation of the centre of gravity of the barge is expressed as follows:

$$\begin{cases}\dot{x}_g = u_b\cos\psi_b - v_b\sin\psi_b - 1\\ \dot{y}_g = u_b\sin\psi_b - v_b\cos\psi_b\\ \dot{\psi}_b = r_b\\ l^2 = (x_g + x_p\cos\psi)^2 + (y_g + x_p\sin\psi)^2\\ \sin\gamma_b = \frac{1}{l}(y_g + x_p\sin\psi_b)\end{cases} \tag{9}$$

where x_g and y_g represent the dimensionless coordinates of the centre of gravity of the barge. In the body-fixed coordinate system, the dynamic loop model of the ship is expressed as follows:

$$\begin{cases}\dot{u}_b = m_{11}{}^{-1}(m_{22}v_br_b + f_u + T_x)\\ \dot{v}_b = -m_{22}{}^{-1}(m_{11}u_br_b + f_v + T_y)\\ \dot{r}_b = m_{33}{}^{-1}((m_{11}-m_{22})u_bv_b + f_r + M_z)\end{cases} \tag{10}$$

where the higher-order hydrodynamic term f is expressed as follows:

$$\begin{cases}f_u = X_uu + X_{|u|u}|u|u + X_{vv}v^2 + X_{rr}r^2 + X_{uuu}u^3\\ f_v = Y_vv + Y_{|v|v}|v|v + Y_{vvv}v^3\\ f_r = N_rr + N_{|r|r}|r|r + N_{rrr}r^3\end{cases} \tag{11}$$

In Eq. (11), owing to the absence of significant interactions between fluid acceleration and inertial forces derived from potential flow theory [8], second-order terms, such as $X_{vv}v^2$ and $X_{rr}r^2$, can be neglected.

The modelling procedure of the tug follows a similar approach and the simplified kinematic loop model is expressed as follows:

$$\begin{cases}\dot{x}_t = u_t\cos\psi_t - v_t\sin\psi_t\\ \dot{y}_t = u_t\sin\psi_t - v_t\cos\psi_t\\ \dot{\psi}_t = r_t\end{cases} \tag{12}$$

In the body-fixed (hull) coordinate system, the dynamic loop model of the tug is expressed as follows:

$$\begin{cases}\dot{u}_t = m_{11}{}^{-1}(m_{22}v_tr_t + f_u + \tau_u - T_x) + d_{wu}\\ \dot{v}_t = -m_{22}{}^{-1}(m_{11}u_tr_t + f_v - T_y) + d_{wv}\\ \dot{r}_t = m_{33}{}^{-1}((m_{11}-m_{22})u_tv_t + f_r + \tau_u - M_z) + d_{wr}\end{cases} \tag{13}$$

where τ_u and τ_r represent the thrust and yaw moment of the tug, respectively, and f denotes the higher-order hydrodynamic term of the tug, expressed in Eq. (11). All related mass parameters and damping coefficients correspond to the tug.

NUMERICAL MODEL OF THE TOWING SYSTEM

To achieve a more accurate representation of the dynamic characteristics of the towing system, and to elucidate the interaction mechanisms between the rope, tug, and barge, a system model was developed to closely mirror real-world conditions. While previous studies addressed various aspects of towing systems, including stability, environmental effects, and towing strategies, highlighting the influence of nonlinearities and external loads, the comprehensive dynamic response of the integrated tug–barge–rope system remains insufficiently characterised. In particular, the coupled mechanical behaviour of these three components under dynamic conditions warrants further investigation through targeted model simulations. This section focuses on the core components of the towing system and establishes three DoF models of the rope, tug, and barge for simulation analysis. The objective was to provide a more intuitive and precise theoretical basis for understanding the dynamic properties of the towing system by quantitatively examining the motion states of these three components. To focus on the inherent effects of rope parameters and avoid external interference, external marine environmental disturbances such as wind, waves and currents, were neglected in the numerical simulations. The initial thrust of the tug was set as 100 Kn and the specific model parameters are listed in Table 1.

Tab. 1 Parameters of the numerical simulation model of the ship towing system

Tug model parameters and initial motion state		
$m_{11} = 120\times10^3\,\text{kg}$	$m_{22} = 177.9\times10^3\,\text{kg}$	$m_{33} = 636\times10^5\,\text{kg}\cdot\text{m}^2$
$X_u = 215\times10^2\,\text{kg}\cdot\text{s}^{-1}$	$X_{\lvert u\rvert u} = 43\times10^2\,\text{kg}\cdot\text{m}^{-1}$	$X_{uuu} = 21.5\times10^2\,\text{kg}\cdot\text{m}^{-2}\text{s}$
$Y_v = 117\times10^3\,\text{kg}\cdot\text{s}^{-1}$	$Y_{\lvert v\rvert v} = 23.4\times10^3\,\text{kg}\cdot\text{m}^{-1}$	$Y_{vvv} = 11.7\times10^2\,\text{kg}\cdot\text{m}^{-2}\text{s}$
$N_r = 802\times10^4\,\text{kg}\cdot\text{m}^2\text{s}^{-1}$	$N_{\lvert r\rvert r} = 160.4\times10^4\,\text{kg}\cdot\text{m}^2$	$N_{rrr} = 80.2\times10^4\,\text{kg}\cdot\text{m}^2\text{s}$
$x = 0\text{m}$	$y = 0\text{m}$	$\psi = 0.1\text{rad}$
$u = 0\text{m/s}$	$v = 0\text{m/s}$	$r = 0\text{rad/s}$
Barge model parameters and initial motion state		
$m_{11} = 500\times10^3\,\text{kg}$	$m_{22} = 560\times10^3\,\text{kg}$	$m_{33} = 636\times10^5\,\text{kg}\cdot\text{m}^2$
$X_u = 608.2\times10^3\,\text{kg}\cdot\text{s}^{-1}$	$X_{\lvert u\rvert u} = 121.6\times10^3\,\text{kg}\cdot\text{m}^{-1}$	$X_{uuu} = 60.8\times10^3\,\text{kg}\cdot\text{m}^{-2}\text{s}$
$Y_v = 327.6\times10^4\,\text{kg}\cdot\text{s}^{-1}$	$Y_{\lvert v\rvert v} = 65.5\times10^4\,\text{kg}\cdot\text{m}^{-1}$	$Y_{vvv} = 32.8\times10^3\,\text{kg}\cdot\text{m}^{-2}\text{s}$
$N_r = 224.6\times10^5\,\text{kg}\cdot\text{m}^2\text{s}^{-1}$	$N_{\lvert r\rvert r} = 449.1\times10^5\,\text{kg}\cdot\text{m}^2$	$N_{rrr} = 22.5\times10^5\,\text{kg}\cdot\text{m}^2\text{s}$
$x = L_0 + 10\text{m}$	$y = 5\text{m}$	$\psi = 0\text{rad}$
$u = 0\text{m/s}$	$v = 0\text{m/s}$	$r = 0\text{rad/s}$
Rope parameters		
$K_{r_0} = 500\times10^2\,\text{N/m}$	$\delta = 0.2$	$l_0 = 20\text{m}$

In order to comprehensively analyse the mechanical behaviour of the tug system under practical operating conditions, the development of an accurate numerical model is essential. Numerical simulation enables the efficient prediction of the dynamic properties of the system under varying loads and environmental conditions, providing a theoretical basis for optimised design, enhanced safety margins, and reduced operational and maintenance costs. In this experiment, the numerical model of the tug system was developed using Matlab software and multi-body dynamics theory, with the objective of delivering reliable technical support for relevant engineering applications. The simulation results are shown in Figs. 3–6.

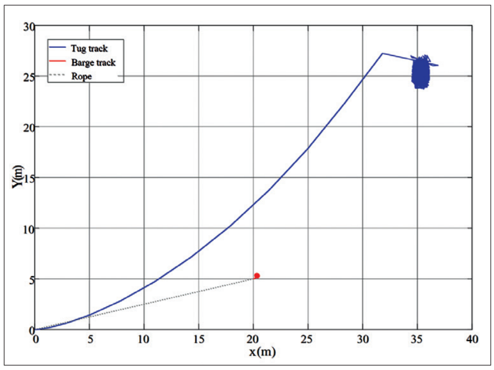

Fig. 3 Simulation trajectories of the ship towing system

The planar motion trajectories of the tug and barge, under the natural-length initial condition of the rope, are shown in Fig. 3. The initial position of the tug was set at the origin and the initial coordinates of the barge were expressed as (l_0, 5), with an initial yaw angle of 0.1 rad. Analysis of the motion characteristics revealed that the tug demonstrated high-frequency, sawtooth-like oscillations with an amplitude of ±3 m, indicating frequent positional adjustments over short time intervals. The barge closely followed the tug, maintaining a lag distance of < 5 m, which demonstrates a rapid response to the movements of the tug. This behaviour was primarily attributed to the relatively high stiffness of the rope, which enforced strong coupling between the tug and barge. Consequently, energy was transmitted efficiently through the rope, enabling the barge to promptly react to changes in the motion of the tug.

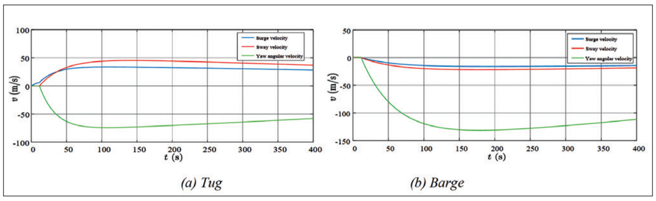

Fig. 4 Time histories of ship motion states

The motion states of the tug and barge, which can be analysed in terms of their surge, sway, and yaw angular velocities, are shown in Fig. 4. As shown in Fig. 4(a), the surge velocity of the tug steadily increased under the influence of thrust and then oscillated, which characterises the acceleration phase of the tug. The sway velocity demonstrated a decaying oscillation, primarily attributed to the combined effects of rope tension and fluid damping. The yaw angular velocity underwent periodic fluctuations, which are indicative of torque imbalances resulting from lateral displacement. Notably, after approximately 100 s, the system demonstrated velocity oscillations, signifying that the tug gradually attained a state of dynamic equilibrium. As shown in Fig. 4(b), the surge velocity of the barge increased at a slower rate, predominantly driven by the towing force transmitted through the rope. Its sway velocity demonstrated large-amplitude oscillations, reflecting the pronounced inertial response owing to the substantial mass of the barge. The yaw angular velocity displayed low-frequency fluctuations, corresponding to the large rotational inertia of the barge. Comparative analysis revealed that the response of the barge lagged behind that of the tug by approximately 15–20 s, further validating the pronounced inertial characteristics of a massive body in motion.

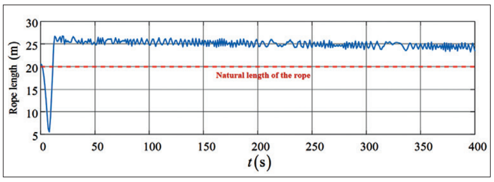

Fig. 5 Time history of rope length in the ship towing system

The dynamic variation of rope length is shown in Fig.Fig. 5. The red line represents the natural length of the rope, $l_0 = 20$ m; whereas, the blue line represents its real-time length. At t = 20 s, the rope experienced its maximum strain value, indicating a significant instantaneous elongation. Importantly, this strain exceeded the safe limit by 20%, highlighting the necessity for careful consideration of material fatigue to ensure the long-term safety and reliability of the rope.

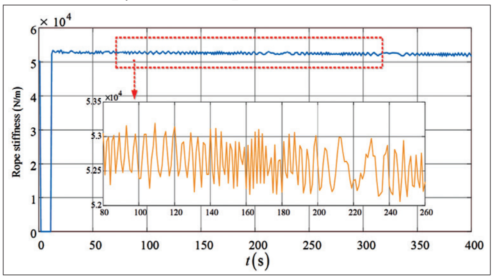

Fig. 6 Time history of rope stiffness in the ship towing system

The stiffness properties of the rope are shown in Fig. 6. Pronounced nonlinear behaviour was observed, with stiffness increasing with the strain. During the slack phase, when the rope length l_0 was less than, or equal to, its initial length, the stiffness was zero, reflecting the relaxed state of the rope. Moreover, the rope demonstrated typical spring-like properties, which are consistent with the theoretical description of nonlinear rope models.

IMPACT OF SYNTHETIC FIBRE ROPE PARAMETERS ON THE TOWING SYSTEM

ROPE LENGTH

In practical applications, the rope serves as the primary connection between the two vessels and influences the dynamic responses of the system. An excessively short rope can intensify impact loads between the ships; whereas, an excessively long rope may lead to uncontrollable oscillatory motions. Therefore, investigating the coupled effects of varying rope lengths on ship motion and rope mechanical behaviour enhances the theoretical understanding of towing system dynamics and provides scientific guidance for the optimal selection of rope parameters in engineering practice.

Fig. 7 presents the time histories of surge velocities for the tug and barge. To clearly distinguish the two vessels, the solid line represents the tug, while the dashed line represents the barge. Quantitative analysis of the impact of different natural rope lengths on rope dynamics indicated that, with increasing rope length, the tug velocity amplitude fluctuations gradually decreased. When $l_0 = 120$ m, the amplitude of the tug velocity amplitude fluctuation was ± 0.3 m/s. However, the response of the barge to the motion of the tug became increasingly delayed, with the lag time extending to > 30 s, and the system required approximately 200 s to reach a steady state. Simulation data further indicated that short ropes are prone to high-frequency resonance. This phenomenon primarily arises because the natural frequency of the system approaches that of wave-induced disturbances, resulting in rapid energy transmission and accumulation within the system. Conversely, long ropes demonstrated pronounced velocity lag, which is attributable to their elastic properties and caused delayed barge responses to tug motion.

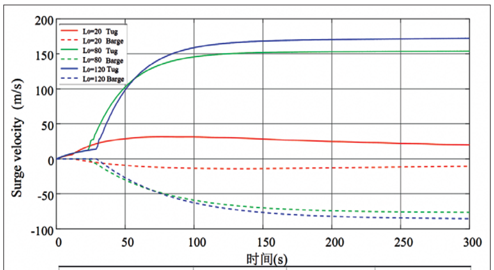

Parameter	l_0=20	l_0=80	l_0=120
Tug speed fluctuation amplitude	±0.8m/s	±0.5m/s	±0.3m/s
Barge velocity lag time	<5s	10-15s	>30s
System setting time	50s	120s	200s

Fig. 7 Variation in ship surge velocity with different rope lengths

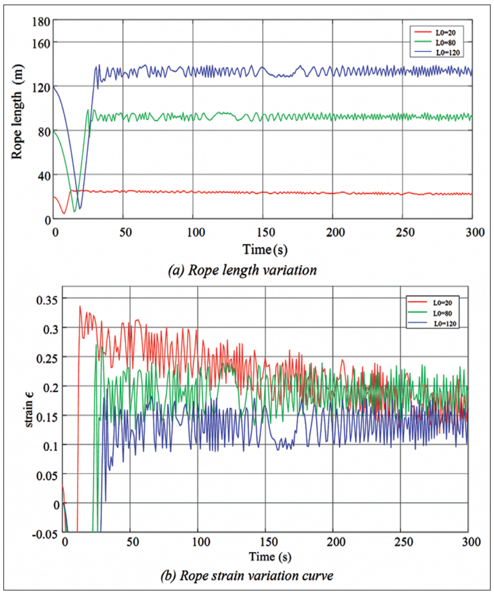

Fig. 8 Variation in rope length during ship navigation

The variation in rope length during ship navigation is shown in Fig. 8. The maximum elongation increased with the natural rope length, as shown in Fig. 8(a). From the simulation data, when $l_0 = 20$ m, the maximum elongation was 6 m, equivalent to 30% of its natural length; when $l_0 = 80$ m, the maximum elongation was 20 m, corresponding to 25% of its natural length; and when $l_0 = 120$ m, the maximum elongation was 17 m, equivalent to

14.2% of its natural length. By integrating the results from Fig. 8(b) with the requirements of the ISO 18682 standard, the safety performance assessment of ropes indicated that the strain satisfied the requirement for long ropes (<18%) when $l_0 = 120$ m. However, when the rope length $l_0 = 20$ m, 80 m the maximum strain exceeded the safety threshold (>20%), indicating a significant risk of rope rupture under such conditions. Meanwhile, as the rope length increased, the dominant oscillation frequency gradually decreased, indicating that longer ropes possess longer vibration periods and slower dynamic responses. During navigation, the strain values for ropes of varying lengths gradually converged to a stable value, indicating that the surface wear-in process became more complete and the microstructures of the material approached stability.

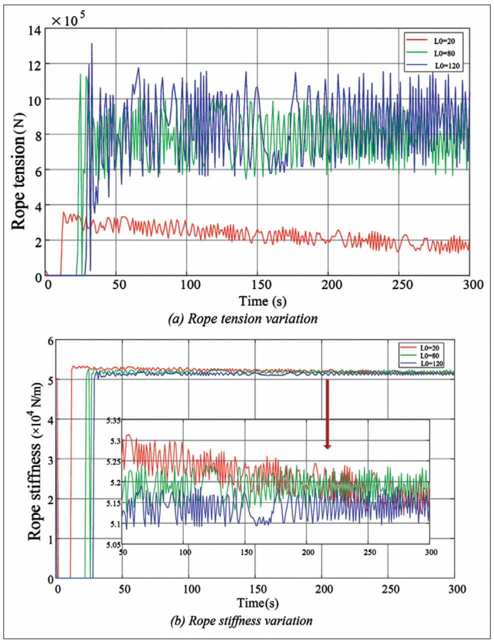

Fig. 9 Variation in mechanical properties of rope during ship navigation

The dynamic properties of rope tension under different initial rope lengths are shown in Fig. 9(a). The simulation results indicated that, in the initial stage, rope tension demonstrated a pronounced nonlinear increase. When $l_0 = 20$ m, the tension rapidly increased from 0 to 4×10^5 N within 10 s, resulting in a steeply rising curve. Next, the tension gradually transitioned into an oscillatory decay phase before ultimately stabilising. Furthermore, the tension curves displayed distinct periodic oscillations with frequencies ranging from approximately 0.2–0.5 Hz, corresponding to oscillation periods of 2–5 s. This oscillatory behaviour reflects the coupled vibration in the tug–barge system, which is a feature of the dynamic response of the system. Furthermore, when $l_0 = 80$ m, 120 m the behaviour was observed at approximately t = 30 s, where the tension suddenly decreased, momentarily reaching zero. This phenomenon occurred when the rope length temporarily became shorter than its initial length ($l \leq l_0$), resulting in slack and a subsequent abrupt change in tension. Such behaviour was attributed to the inherent lag in the dynamic response of the rope system: when the external load changed rapidly, inertial effects within the system prevented the tension from being immediately balanced, resulting in this transient phenomenon. As shown in Fig. 9(b), the rope stiffness also experienced a sharp decline to zero during this period. However, data comparison indicated that the stiffness peak lagged the tension by approximately 0.5 s, owing to stiffness updates governed by variations in the rope length. The rope stiffness is primarily determined by the strain ε. Under varying initial length conditions, the dynamic response of rope stiffness displayed significant variations. For short ropes, the initial stiffness was approximately 5.34×10^5 N (approximately 11% higher than the natural stiffness k_0), indicating that the rope was subjected to greater tensile loading in the initial phase. Subsequently, the stiffness gradually decreased over time and stabilised. In contrast, long ropes displayed more gradual stiffness variations, making them better suited for applications requiring higher operational precision.

The analysis of the dynamic properties of the towing system clearly demonstrated that the rope length impacts system behaviour. Specifically, systems with short ropes ($l_0 = 20$ m) tended to demonstrate pronounced nonlinear characteristics, greater relative deformation, and more significant stiffness variations, resulting in more intense dynamic responses. Accordingly, their initial working conditions must be strictly controlled and material toughness must be enhanced to withstand potential failures. Conversely, systems with long ropes ($l_0 = 120$ m) experienced milder dynamic variation, larger absolute displacements, and slower energy dissipation processes, whilst also being more sensitive to initial conditions. Although long ropes displayed lower strain values, attention must be paid to cumulative fatigue effects in long-term service. This necessitates the regular inspection and adjustment of slack cycles, to ensure sustained performance stability. For medium-length ropes ($l_0 = 80$ m), the design must achieve an optimal balance between dynamic response and safety performance, to ensure reliability under various operating conditions. Furthermore, the interactions between subsystems highlight the complexity of the towing system: the thrust of the tug and rope tension formed a dynamic equilibrium; whereas, the inertia of the barge resulted in delayed responses. The nonlinear stiffness of the rope is crucial in regulating system behaviour, resulting in characteristic underdamped vibration phenomena. These insights elucidate the intricate dynamic behaviour of the multi-body towing system and provide a robust theoretical foundation for optimising rope parameters and developing advanced system control strategies. Such findings offer valuable guidance for system design and performance optimising practical engineering applications.

ROPE MATERIAL

In rope towing systems, the mechanical properties of the rope material directly impact system stability, energy efficiency, and operational safety. In this study, three widely used rope materials (nylon, polyester, and ultra-high-molecular-weight polyethylene (UHMWPE)) were selected for analysis. Their respective material parameters and engineering properties are listed in Table 2.

Tab. 2. Material parameters and engineering properties of three synthetic fibre ropes

Material name	Initial stiffness K_{r_0} (N/m)	Nonlinear coefficient δ	Engineering properties
Nylon	2×10^4	0.3	Excellent elasticity and high toughness, with favourable impact resistance and fatigue life.
Polyester	5×10^4	0.2	Medium strength, superior creep resistance compared with nylon, and good weather resistance.
UHMWPE	2×10^5	0.31	Long molecular chains with tight alignment, high strength, and low density (lighter than water).

A dynamic model of the rope towing system was established and validated through simulations, to compare the performance of these three materials under actual operating conditions. The model utilised the thrust of the tug 1×10^5 N as input and simulated the dynamic response of the system over a 0–100 s interval, incorporating an initial 3 m lateral offset of the barge as a disturbance. Core ship parameters were consistent with those listed in Table 1. By quantifying dynamic parameters, such as rope elongation, tension, and stiffness, alongside system-level indicators including tug velocity and barge yaw angle, a comprehensive evaluation of the impact of material properties on overall system performance was conducted.

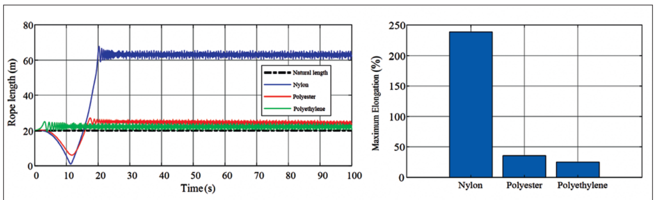

Fig. 10. Comparison of actual length and elongation of synthetic fibre towing ropes

The rope elongation serves as a key metric for characterising the degree of elastic deformation during towing, directly reflecting the flexibility of each material. As shown in Fig. 10, the length variations for all materials demonstrated a pattern of rapid initial growth–stable peak–gradual convergence, corresponding to the transition of a system from a transient to a steady state. The observed trends in length variation aligned closely with the inherent elongation properties of each material. The nylon rope demonstrated the highest ratio of maximum length to natural length; whereas, UHMWPE demonstrated the lowest. Owing to its lower initial stiffness (K_{r_0} 2×10^4), the nylon rope also displayed a significantly higher peak elongation rate compared with those of the other materials. Nylon, characterised by its pronounced flexibility, effectively absorbed system disturbance energy through substantial deformations. The polyester rope presented an intermediate elongation rate, with deformation capacity positioned between that of nylon and UHMWPE. Conversely, UHMWPE ropes, owing to their highest initial stiffness (K_{r_0} 2×10^5), displayed minimal elongation and the lowest fluctuation amplitude, demonstrating prominent stiffness. Additionally, as the rope stiffness increased, the fluctuation frequency of the decreased, indicating that stiffer materials can attenuate high-frequency, sawtooth-like oscillations. Notably, under the present simulation conditions, nylon towing ropes demonstrated relatively large elongations (with breaking elongation typically ranging from 20–400%, approaching 500% in some cases of low-crystallinity nylon), requiring further investigation.

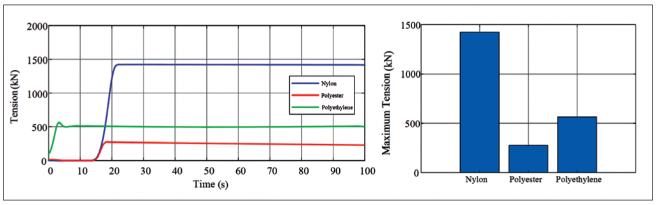

Fig. 11. Time history of tension in synthetic fibre towing ropes

From a physical perspective, the tensile load of the rope directly reflects the mechanical performance of the material and serves as a critical parameter for evaluating strength and system safety. As shown in Fig. 11, the three materials demonstrated distinct mechanical behaviours. The UHMWPE rope, owing to its high stiffness, demonstrated the smallest elongation but generated an elastic force significantly higher than that of polyester, resulting in the most pronounced initial tension peak. The polyester rope demonstrated an intermediate tension response with reduced fluctuations, offering a favourable balance between stiffness and damping. Conversely, the nylon rope, consistent with its elongation characteristics (Fig. 10), experienced the largest tension. A comparison between polyester and UHMWPE revealed that, although high-stiffness materials undergo less deformation, the tension generated per unit deformation is substantially higher, thereby imposing more stringent strength requirements on the material.

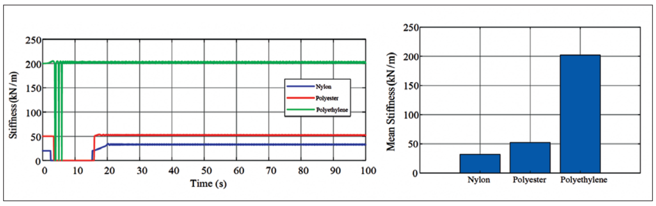

Fig. 12 Time history of the stiffness of synthetic fibre towing ropes

The variation in rope stiffness reflects the nonlinear mechanical behaviour of materials during deformation and serves as a foundation for characterising their dynamic mechanical properties. Significant differences were observed in the stiffness variation trends among the materials (Fig. 12). The UHMWPE rope consistently maintained the highest stiffness level, displaying a nonlinear increase with elongation; its average stiffness was significantly greater than those of the other materials. The stiffness curve for the polyester rope occupied an intermediate position, with a growth rate surpassing that of UHMWPE. In contrast, the nylon rope, despite experiencing the most significant deformation, demonstrated the lowest dynamic stiffness. The order of the materials' dynamic stiffness was as follows: UHMWPE (approximately 220 kN/m) > polyester (approximately 60 kN/m) > nylon (approximately 30 kN/m). Furthermore, during the initial phase when the rope length was less than its natural length (a brief slack condition), the theoretical stiffness value was zero. This stage, which is not represented in the simulation curves, indicates that the rope had not yet entered the load-bearing state.

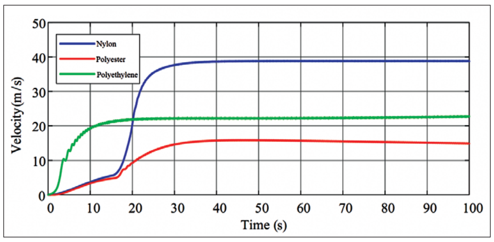

Fig. 13 Time history of the synthetic velocity of towing ropes made of synthetic fibres

In the context of power transmission within the towing system, the physical properties of the rope material are crucial in determining the efficiency of energy transfer. The simulation results presented in Fig. 13 indicate that the UHMWPE rope outperformed the polyester rope, in terms of power transmission, as evidenced by the highest average tug velocity. This superior performance was attributed to the higher stiffness of UHMWPE, which minimises elastic deformation under load and thereby enhances energy transfer efficiency. Consequently, energy dissipation during rope deformation was significantly reduced, leading to enhanced overall power transmission efficiency within the system. In comparison, the nylon rope achieved the highest velocity, which can probably be attributed to its ability to undergo substantial deformation, which cushions initial impacts and reduces reverse tension. Coupled with its low damping characteristics, nylon minimises power loss and enables more efficient conversion of thrust into velocity. This outcome highlights the inherent trade-off between "material flexibility and power efficiency" in towing systems. Notably, the velocity profiles for all tested materials stabilised after approximately 50 s, indicating the onset of a steady towing phase. During this period, the observed velocity differences between the materials were primarily attributed to their distinct energy dissipation behaviours under steady conditions.

The mechanical properties of each rope material determine their suitability for towing applications. Simulation results indicated that the UHMWPE ropes are well-suited for scenarios demanding high system stability and power transmission efficiency. The high stiffness of UHMWPE effectively suppresses barge yaw motion and substantially limits dynamic rope deformation, thereby minimising energy dissipation and enhancing towing efficiency. However, the relatively low elastic modulus of UHMWPE diminishes its ability to absorb sudden impact loads, potentially resulting in elevated peak stresses within the system when exposed to abrupt external forces.

The polyester rope demonstrated strong overall performance, achieving an optimal balance between elongation, tensile strength, and system stability. Its moderate elasticity enables the rope to effectively accommodate typical towing conditions while maintaining high towing efficiency and ensuring a robust level of safety. These characteristics make polyester ropes particularly well-suited to long-duration operations under medium-load conditions.

In contrast, the nylon rope demonstrated superior elastic buffering capacity, allowing it to absorb significant impact energy. However, its high elongation adversely impacts system stability, as the dynamic stretching and contraction of the rope require additional tug power, thereby reducing overall towing efficiency. Therefore, the nylon ropes are more appropriate for applications where buffering capability is prioritised over operational efficiency.

This analysis underscores the importance of selecting rope materials based on the specific operational environment and performance requirements, in order to achieve an optimal balance between stability, efficiency, and impact resistance.

CONCLUSIONS

This study addressed the core challenges associated with the absence of parameter design theory and the complexities of stability regulation for synthetic fibre ropes in marine towing system applications. By developing a multi-body coupled mathematical model of a tug–barge–rope system, a comprehensive quantitative investigation was conducted to evaluate the influence of rope length and material properties on the dynamic performance of the towing system. The major findings of the study are summarised below.

Regarding the optimisation of rope length parameters, this study identified a nonlinear correlation between the rope length and system dynamic response. A short rope of 20 m, owing to its limited capacity for elastic deformation, subjected the power system of the tug to instantaneous overloads. Its heightened strain sensitivity induced high-frequency, sawtooth-like tension fluctuations, significantly increasing the risk of rope fatigue damage. In contrast, an 80 m medium-length rope leveraged the viscoelastic properties of its material to effectively dissipate wave energy, achieving an optimal balance between tension fluctuation amplitude and motion stability. Conversely, a 120 m long rope experienced stiffness attenuation, resulting in a barge motion phase lag exceeding 30 s. While this configuration effectively buffered the impacts of rapid acceleration and deceleration of the tug, it also introduced a risk of system instability, owing to dynamic lag. These findings provide a quantitative foundation for selecting appropriate rope lengths across various operational scenarios, thereby addressing the limitations inherent in conventional empirical designs.

Regarding material performance adaptation, this study elucidated the distinct mechanical regulation mechanisms of different synthetic fibre materials. Nylon ropes, characterised by a high elastic modulus, facilitated rapid tension transmission under short-rope configurations, making them well-suited for emergency towing scenarios that demand a swift response. Polyester fibres, with their high damping properties, effectively suppressed vortex-induced vibrations in medium-length rope applications. UHMWPE ropes, noted for their exceptional strength-to-weight ratio, provided lightweight solutions for long-rope applications under heavy-load conditions. Collectively, these results establish systematic criteria for matching material properties, rope configurations, and operational requirements.

This study addressed three core areas: graded length selection, material-oriented adaptation, and dynamic control. Future research will prioritise the development of a comprehensive rope parameter design atlas and predictive models of system dynamic performance, aiming to significantly reduce design cycles and mitigate operational risks. This study not only advances the theoretical framework for the application of synthetic fibre ropes in marine towing systems but also provides key technical support for the development of deep-sea engineering equipment. Future studies will investigate multi-physics coupling effects under extreme sea conditions, further enhancing the engineering applicability of the model.

REFERENCES

1. Ma J, Shi J, Lian Y, Zheng J, Zhang J, Liu T, Chen W. Experimental study on creep and abrasion properties of polyester yarns for deep-sea mooring applications. Ocean Engineering 2025, 341, 122774. https://doi.org/10.1016/j.oceaneng.2025.122774.

2. Zhang H, Zeng J, Tong, S, Jin B, Chou C, Li H, Dong H. Dynamic stiffness of polyester fiber mooring ropes: Experimental investigation based on radial basis function neural networks [J]. Ocean Engineering 2023, 280, 114833. https://doi.org/10.1016/j.oceaneng.2023.114833.

3. Lian Y, Zhang Y, Zheng J, Zhang J, Chen W, Chen S, Wu X, Xie Y, Ma J, Liu H, Yim SC. Experimental investigation on dynamic stiffness of full-scale polyester mooring ropes. Ocean Engineering 2025, 332, 121403. https://doi.org/10.1016/j.oceaneng.2025.121403.

4. Kontou E, Spathis G, Georgiopoulos P. Modeling of nonlinear viscoelasticity-viscoplasticity of bio-based polymer composites [J]. Polymer Degradation and Stability 2014, 110, 203-207. https://doi.org/10.1016/j.polymdegradstab.2014.09.001.

5. Zhang H, Zeng J, Jin B, Chou C, Li H, Dong H. Experimental Study of the Nonlinear Behaviour of Deep-Sea Mooring Polyester Fibre Ropes [J]. Polish Maritime Research 2023, 30, 153–62. https://doi.org/10.2478/pomr-2023-0048.

6. Xie Y, Lian Y, Zheng J, Zhang J, Xue M-A, Wu X, Gao C, Liu T, Yim SC. Experimental investigation on the quasi-static and dynamic stiffness of full-scale HMPE ropes. Ocean Engineering 2025, 342, 123002. https://doi.org/10.1016/j.oceaneng.2025.123002.

7. Wu J-T, Chen, J-H, Hsin C-Y, Chiu F-C. Dynamics of the FKT System with Different Mooring Lines. Polish Maritime Research 2019, 26 (1), 20–29. https://doi.org/10.2478/pomr-2019-0003.

8. Bernitsas MM, Kekridis NS. Simulation and stability of ship towing. Int. Shipbuild. Progr. 1985, 32 (369), 112–123. https://doi.org/10.3233/ISP-1985-3236901.

9. Bernitsas MM, Kekridis NS. Nonlinear stability analysis of ship towed by elastic rope. J. Ship Res. 1986, 30, 136–146. https://doi.org/10.5957/jsr.1986.30.2.136.

10. Lee ML. Dynamic stability of nonlinear barge-towing system. Appl. Math. Model 1989, 13 (12), 693–701. https://doi.org/10.1016/0307-904X(89)90162-5.

11. Bernitsas MM, Chung JS. Nonlinear stability and simulation of two-line ship towing and mooring. Appl. Ocean Res. 1990, 12 (2), 77–92. https://doi.org/10.1016/S0141-1187(05)80032-X.

12. Kijima K, Varyani K. Wind effect on course stability of two towed vessels. J. Soc. Nav. Archit. Jpn. 1985, (158), 137–148. https://doi.org/10.2534/jjasnaoe1968.1985.158_137.

13. Fitriadhy A, Yasukawa H, Koh KK. Course stability of a ship towing system in wind. Ocean Eng. 2013, 64, 135–145. https://doi.org/10.1016/j.oceaneng.2013.02.001.

14. Huang W, Li B, Kim DK. An investigation on material diversity of synthetic fibre ropes in the course stability of towing under wind. Ocean Eng. 2023. https://doi.org/10.1016/j.oceaneng.2023.114410.

15. Cao X, Zhou Z, Zhang H, Zhang N. A review on the stability of towed floating bodies during wet towing operations. Ocean Eng. 2017, 340. https://doi.org/10.1016/j.oceaneng.2025.122449.

16. Roberts A, Le Pivert F, Kazemi S, Tosdevin T, López-Santander A, Craven MJ, Johanning L. Scale model and ship simulator towing of the IEA 15MW wind turbine on the UMaine VolturnUS-S platform. Ocean Eng. 2025, 336. https://doi.org/10.1016/j.oceaneng.2025.121732.

17. Kim B, Kim TW. Weather routing for offshore transportation using genetic algorithm. Appl. Ocean Res. 2017, 63, 262–275. https://doi.org/10.1016/j.apor.2017.01.015.

18. Szlapczynska J, Szlapczynski R. Preference-based evolutionary multi-objective optimization in ship weather routing. Appl. Soft Comput. 2019, 84. https://doi.org/10.1016/j.asoc.2019.105742.

19. Le Pivert F, López-Santander A, Craven MJ, Roberts A. Routing optimisation for towing a floating offshore wind turbine under weather constraints. Ocean Eng. 2024, 305, 0029–8018. https://doi.org/10.1016/j.oceaneng.2024.118025.

20. Le Pivert F, Roberts A, López-Santander A, Craven MJ, Kazemi S. Data driven multi-objective optimization of the scheduling for towing a floating offshore wind turbine between assembly port and installation location throughout a year. Appl. Ocean Res. 2025, 157, 0141–1187. https://doi.org/10.1016/j.apor.2025.104492.

21. Zhang X, Jia X. Ship motion control. National Defense Industry Press; 2006.